captures the evolution of a complex adaptation on a much finer scale. We used a relaxed molecular clock approach (*10*, *15*, *16*) to estimate the time required for extensive maternal provisioning to evolve in *P. turneri*, *P. presidionis*, and *P. prolifica*. Our point estimates are 2.36 and 0.75 million years ago for the "mostly southern" and "mostly northern" species, respectively (*10*). These time intervals estimate the maximum time available for the evolution of extensive maternal provisioning. The actual time is less than or equal to these intervals. It is thus clear that complex adaptations can evolve rapidly, on the same scale as theorized by Nilsson and Pelger (*2*) for the evolution of eyes.

The more important feature of these results is the scope of variation that is present within a group of closely related organisms and hence the potential for using these fish to study the evolution of novelty and complexity. Given the likely complexity of the adaptations associated with extensive maternal provisioning, this range of variation in *Poeciliopsis* is comparable to finding a single genus that has three independent origins of elaborate eyes, including congeners that have either no eyes or eyes in various intermediate stages of evolution.

The availability of three separate clusters of extensive maternal provisioning and the ability of some of these species to hybridize with one another (*17*, *18*) provide the necessary raw material for evaluating the repeatability of the underlying mechanisms that generate this adaptation. For example, the subgenus *Poeciliopsis* includes the species that hybridize in nature to produce hybridogenetic and gynogenetic clones. Additional hybrids have been produced artificially (*17*, *18*). A compelling feature of these hybridizations is that the female partner is always *P. monacha* (*19*), which has no post-fertilization maternal provisioning (Fig. 3) and hence is insulated from many aspects of intergenomic conflict. Furthermore, there are other species scattered throughout the family Poeciliidae that have either moderate or extensive amounts of maternal provisioning (*20*, *21*). Although phylogenetic relationships among the rest of the family have yet to be resolved in comparable detail to the genus *Poeciliopsis*, there clearly are additional opportunities to evaluate independent origins of placentas. The extensive literature on placental reproduction in mammals provides guidance for the kind of adaptations one might find when evaluating a similar adaptation in fish. Experimentally accessible phenomena in Poeciliidae might include the progressive development of the genetic and morphological mechanisms associated with maternal provisioning or the escalating intergenomic conflict associated first with egg retention and then with the increasing commitment of maternal resources after fertilization. These adaptations cannot be directly studied or manipulated in placental mammals, because their placentas are derived from a common ancestor that lived more than 100 million years ago and because the intermediate stages associated with this adaptation have long since been lost through extinction.

References and Notes

1. C. Darwin, *The Origin of Species by Means of Natural Selection* (John Murray, London, 1859).
2. D.-E. Nilsson, S. Pelger, *Proc. R. Soc. London Ser. B* **256**, 53 (1994).
3. D. G. Blackburn, in *Encyclopedia of Reproduction*, E. Knobil, J. D. Neill, Eds. (Academic Press, San Diego, CA, 1999), vol. 3, pp. 840–847.
4. J. Rossant, J. C. Cross, *Nature Rev. Genet.* **2**, 538 (2001).
5. D. Haig, *Q. Rev. Biol.* **68**, 495 (1993).
6. S. Handwerger, in *Encyclopedia of Reproduction*, E. Knobil, J. D. Neill, Eds. (Academic Press, San Diego, CA, 1999), vol. 3, pp. 855–863.
7. R. E. Thibault, R. J. Schultz, *Evolution* **32**, 320 (1978).
8. C. L. Turner, *J. Morphol.* **67**, 59 (1940).
9. J. P. Wourms, B. D. Grove, J. Lombardi, in *Fish Physiology*, W. S. Hoar, Ed. (Academic Press, London, 1988), vol. 8, pp. 2–134.
10. Materials and methods are available as supporting material on *Science* Online.
11. T. W. Sadler, Ed., *Langman's Medical Embryology* (Williams & Wilkins, Baltimore, MD, ed. 7, 1995).
12. M. Mateos, O. I. Sanjur, R. C. Vrijenhoek, *Evolution* **56**, 972 (2002).
13. D. E. Rosen, R. M. Bailey, *Bull. Am. Mus. Nat. Hist.* **126**, 1 (1963).
14. N. Goldman, J. P. Anderson, A. G. Rodrigo, *Syst. Biol.* **49**, 652 (2000).
15. J. L. Thorne, H. Kishino, I. S. Painter, *Mol. Biol. Evol.* **15**, 1647 (1998).
16. H. Kishino, J. L. Thorne, W. J. Bruno, *Mol. Biol. Evol.* **18**, 352 (2001).
17. R. J. Schultz, in *Ecology and Evolution of Livebearing Fishes (Poeciliidae)*, G. K. Meffe, F. F. J. Snelson, Eds. (Prentice Hall, Englewood Cliffs, NJ, 1989), pp. 69–88.
18. D. Wetherington, R. A. Schenck, R. C. Vrijenhoek, in *Ecology and Evolution of Livebearing Fishes (Poeciliidae)*, G. K. Meffe, F. F. J. Snelson, Eds. (Prentice-Hall, Englewood Cliffs, NJ, 1989), pp. 259–276.
19. R. C. Vrijenhoek, *J. Hered.* **84**, 388 (1993).
20. D. N. Reznick, D. B. Miles, in *Ecology and Evolution of Livebearing Fishes (Poeciliidae)*, G. K. Meffe, F. F. J. Snelson, Eds. (Prentice-Hall, Englewood Cliffs, NJ, 1989), pp. 125–148.
21. A.-L. Arias, D. N. Reznick, *Copeia* **2000**, 792 (2000).
22. J. L. Haynes, *Copeia* **1995**, 147 (1995).
23. R. R. Sokal, F. J. Rohlf, *Biometry* (Freeman, New York, ed. 2, 1981).

24. Supported by the NSF (Research Experiences for Undergraduates supplements, Systematic Biology, Population Biology) and the Academic Senate of the University of California. The University of Michigan, American Museum of Natural History, Smithsonian Institution, and Academy of Natural Sciences of Philadelphia allowed D.N.R. access to their collections. S. Pearson dissected many of the specimens. D. Elder entered and edited data. C. Ghalambor prepared Figs. 1 and 2. The Reznick lab group critically reviewed the manuscript. R.Vrijenhoek provided DNA samples. We dedicate this paper to the memory of John A. Moore.

Supporting Online Material

www.sciencemag.org/cgi/content/full/298/5595/1018/DC1
Materials and Methods
Supporting Text
Figs. S1 and S2
Table S1
References and Notes

11 July 2002; accepted 9 September 2002

Waves of Larch Budmoth Outbreaks in the European Alps

Ottar N. Bjørnstad,[1]* Mikko Peltonen,[2] Andrew M. Liebhold,[2] Werner Baltensweiler[3]

Spatially extended population models predict complex spatiotemporal patterns, such as spiral waves and spatial chaos, as a result of the reaction-diffusion dynamics that arise from trophic interactions. However, examples of such patterns in ecological systems are scarce. We develop a quantitative technique to demonstrate the existence of waves in Central European larch budmoth (*Zeiraphera diniana* Gn.) outbreaks. We show that these waves travel toward the northeast-east at 210 kilometers per year. A theoretical model involving a moth-enemy interaction predicts directional waves, but only if dispersal is directionally biased or habitat productivity varies across the landscape. Our study confirms that nonlinear ecological interactions can lead to complex spatial dynamics at a regional scale.

There is growing evidence that animal population dynamics are governed by nonlinear processes capable of producing a variety of temporal patterns, including equilibrium dynamics, regular oscillations, and even chaotic dynamics (*1*, *2*). When the corresponding nonlinear population models are embedded in spatial landscapes, they often predict a range of complex ("self-organized") spatial dynamics varying from perfect synchrony ("nonlinear phase-locking") to static "crystal lattices," spiral waves, and "spatial chaos" (*3*–*6*). Although there has been considerable success in confirming the existence of these emergent

[1]Departments of Entomology and Biology, 501 ASI Building, Pennsylvania State University, University Park, PA 16802, USA. [2]USDA Forest Service, 180 Canfield Street, Morgantown, WV 26505, USA. [3]Blumenbergstrasse 9, CH-8634 Hombrechtikon, Switzerland.

*To whom correspondence should be addressed. E-mail: onb1@psu.edu

space-time patterns in physical and chemical reaction-diffusion systems, there are few data documenting complex spatial dynamics in ecological systems. Apart from transient invasion waves (*7*), there are few instances of complex spatial dynamics where the data are unequivocal and the underlying mechanisms are well understood. Notable examples are the "Turing patch" (comparable to crystal lattice formation) in the Western tussock moth (*8–10*), traveling waves in the Canadian lynx (*11, 12*), and recurrent waves in several host-pathogen systems such as rabies (*4, 13*) and measles (*14*). Here, we demonstrate recurrent directional (planar) waves in a natural insect population at the landscape scale.

A natural starting point in the search for complex spatial dynamics is among populations that exhibit cyclic oscillations, because they are likely to be governed by highly nonlinear local interactions. Few animal populations exhibit oscillations as regular as those of the larch budmoth (*Zeiraphera diniana* Guenee, syn. *Z. griseana* Hübner) (*15, 16*). Larch budmoth outbreaks have recurred in the European Alps every 8 to 9 years for more than a century, and high population densities cause extensive defoliation of larch forests (*16–18*). In 1964, Baltensweiler (*19*) began to collect space-time data to understand the outbreak dynamics and to document apparent waves in defoliation in this system. We analyzed the 135 time series covering four decades of detailed annual maps of larch budmoth defoliation across the Alps that have resulted from this effort (Fig. 1) (fig. S1) (*20*). Comparison of defoliation and actual population time series indicates that defoliation is a valid indicator of abundance (fig. S2) (*16–18*).

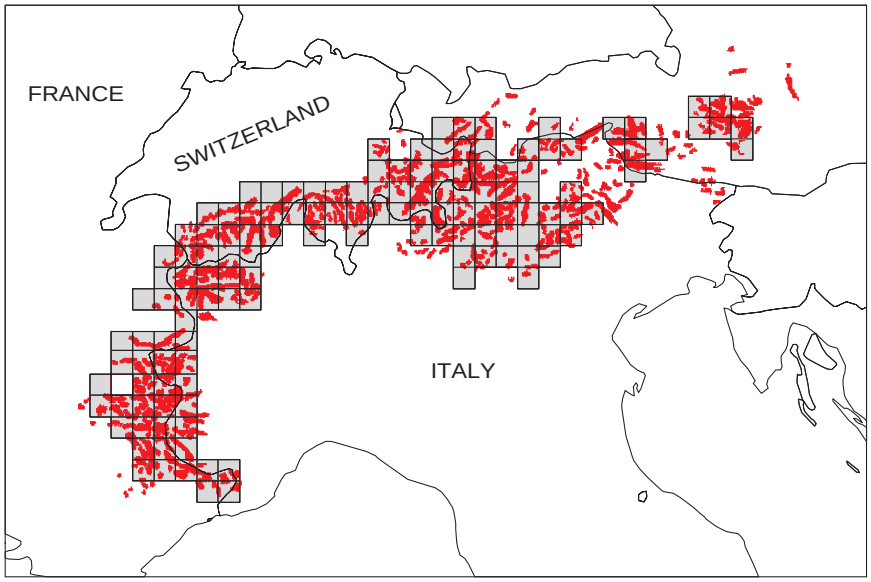

Fig. 1. Historical records of defoliation caused by the larch budmoth in the European Alps (1961 to 1998). Red dots correspond to areas with one or more years of detectable defoliation. The grid shows the location of the 20 km × 20 km aggregates used in the analyses (*18*).

Complex spatial dynamics are associated with characteristic patterns of spatial correlation (*21*). A traveling wave, in particular, is characterized by peak abundance in consecutive years that is offset by a distance corresponding to the wave speed in the cardinal direction of the traveling wave. Thus, a lagged cross-correlation function (LCCF)—the function that describes how the cross-correlation between a spatial variable in successive years is a function of distance (and possibly direction)—of abundance has a mode away from the origin with maximum correlation in the direction of the wave. To estimate the LCCF, we modified the nonparametric covariance function (*21, 22*) to measure the correlation between abundances lagged in time and space (*23*). The LCCF revealed a directional (planar) wave of larch budmoth outbreaks moving across the Alps (Figs. 2 and 3). At time lag 0, spatial correlation generally decreased with increasing distance, irrespective of cardinal direction. Spatial cross-correlation functions at time lags 1 to 3, in contrast, revealed considerable directionality. The wave speed (measured as

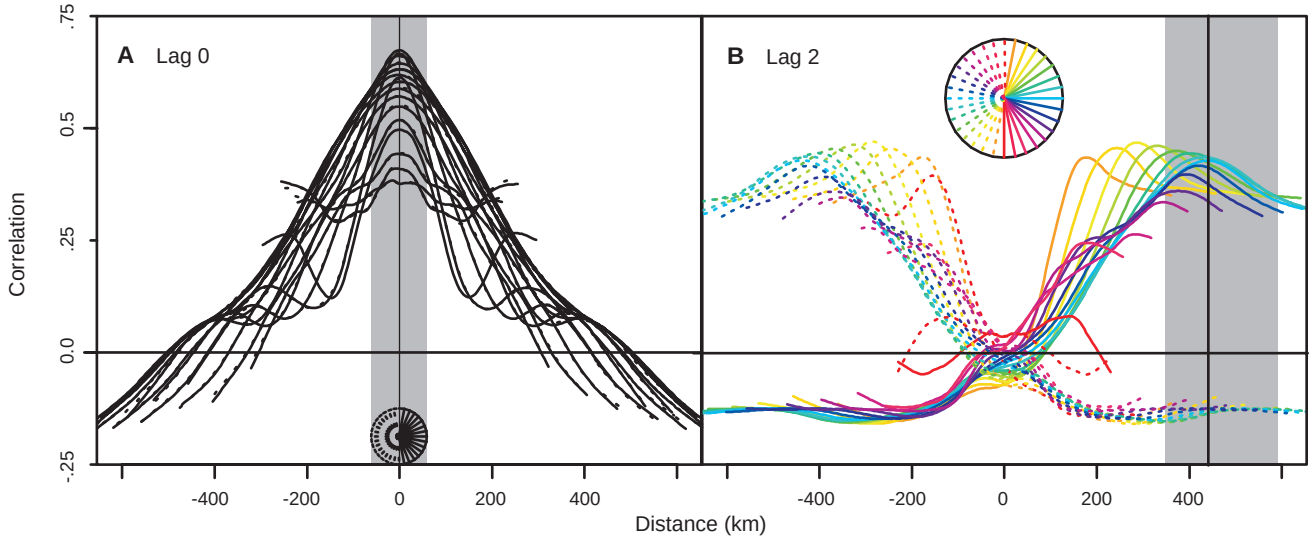

Fig. 2. The lagged cross-correlation function (LCCF) at (**A**) time lag 0 (years) and (**B**) time lag 2 for the larch budmoth data. Easterly LCCFs ($0° \leq \theta < 180°$) are solid lines; westerly LCCFs ($180° \leq \theta < 360°$) are dashed lines (as signified by the compass). In (B), the different directions are signified by varying colors (see compass). Note that in (A), easterly and westerly LCCFs are identical. The mode with confidence interval for maximum correlation is indicated by the vertical bar and gray shading: (A) 0 km {–59.0 km, 59.0 km}, (B) 439.5 km {347.7 km, 597.0 km}. The lag-2 LCCF corresponds to an east-northeast wave (79°) traveling at 219.8 km/year ($CI_{95\%}$ = {173.9, 298.5}). The corresponding estimate based on the lag-1 LCCF (not shown) is an east-northeast wave (67.5°) traveling 203.4 km/year ($CI_{95\%}$ = {137.8, 286.9}).

the distance of peak correlation in the LCCF) was estimated at 219.8 km/year [95% confidence intervals ($CI_{95\%}$) = {173.9, 298.5}; Fig. 2] with a direction northeast-east (65° to 80° from north). The directional waves appear to have their focus at the western border of the core distribution. These waves are conspicuous in fig. S1 (*18*).

The cycles in the larch budmoth population are believed to arise from highly nonlinear trophic interactions between the moth and its parasitoids (*24, 25*) and/or plant quality (*15*). Dispersal by the moth is further thought to be a key process (*16*). Turchin (*25*) developed a set of models embracing the various trophic interactions. A model involving a guild of parasitoids parasitizing the larch budmoth larvae was found to approximate the local cycles (although the other models were found to provide viable alternatives). We used a parasitoid-host coupled-map lattice model to shed light on the directional waves in the larch budmoth (*26*). The local dynamics resulting from the spatially explicit model are cyclic, with a period of just under a decade, as observed in the defoliation records. However, beyond capturing the population cycles, the spatial embedding adds a range of self-organized dynamical patterns to the parasitoid-host interactions. The type of spatial dynamics depended on the absolute and relative mobility of the moth and the parasitoid, indicating the nontrivial role of dispersal (Fig. 4) (fig. S3). With isotropic (nondirectional) dispersal in a homogeneous environment, the host-parasitoid model can lead to nonlinear phase-locking [all population cycles locked into phase (*27*)], radial waves, or spatially chaotic fluctuations. Directional waves, however, do not easily result from this model.

Advective (directional) dispersal has been suggested as a potential cause of the waves in larch budmoth because this moth is a strong flyer capable of mass migrations over long distances. Wind speed and wind direction affect the timing, orientation, and range of such dispersal (*16*). In our models, we found that directional waves—qualitatively similar to those observed in the larch budmoth data—can result from advective moth dispersal. However, such behavior is limited to very narrow parameter ranges for the moth and parasitoid mobilities (Fig. 4B). The spatial dynamics in this model are robust to the magnitude of advection but are sensitive to moth and parasitoid mobility (Fig. 4B) (fig. S3) (*18*). Because of the sensitivity of the spatial dynamics in the moth-parasitoid model, we also explored the alternative trophic model involving feedbacks with plant quality. The resultant spatial dynamics were characterized by spiral or radial waves for all ranges of moth mobility (spiral waves for $0.05 < \mu_h < 0.25$, radial waves for $0.25 < \mu_h < 1$, where μ_h is moth mobility). Directional waves can occur in the presence of advective dispersal. However, the waves invariably traveled in the direction opposite to that of dispersal. Thus, under the moth-plant model, the easterly moth dispersal observed by Baltensweiler and Rubli (*16*) cannot easily cause the easterly directional waves present in the larch budmoth outbreaks. We also considered a host-parasitoid model in a heterogeneous landscape (*26*) so that the dynamics of the moth are governed by a gradient (east-to-west) in habitat quality. This resulted in directional waves (west-to-east) for a wide range of model parameters (Fig. 4C) (fig. S4). Although we do not have any functional candidate for a cline in habitat quality, the model's robustly predicted directional waves may make this idea worthy of further study.

Forty years of detailed spatiotemporal surveys of defoliation caused by the Larch budmoth testify to conspicuous directional waves in the space-time dynamics of this system. These waves travel at 219.8 km/year ($CI_{95\%}$ = {173.9, 298.5}) across the European Alps in a 67° to 80° direction (from the western perimeter of larch forest distribution). Although details need to be resolved, spatiotemporal models broadly predict that waves in defoliation should occur in the larch budmoth system. Our study thus carries two important messages. First, traveling waves are confirmed in an outbreaking insect system. Second, spatially explicit representations of the dominant population processes result in models that qualitatively predict the space-time dynamics.

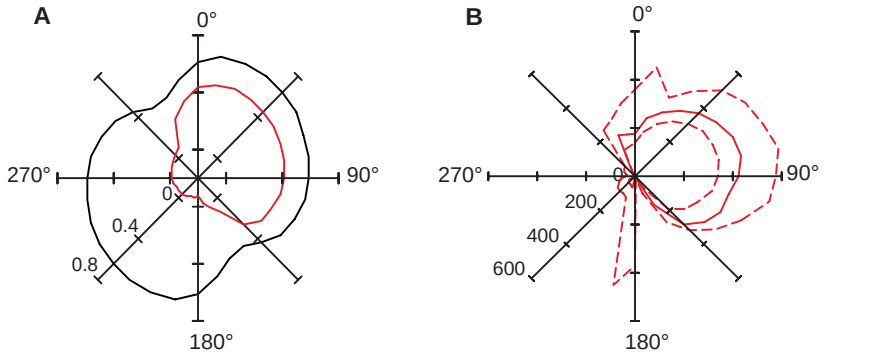

Fig. 3. Maximum LCCF values. (**A**) Maximum correlation for the LCCF for varying directions at time lag = 0 (black) and time lag = 2 years (red). (**B**) Distance of maximum LCCF for each direction (dashed lines are the 95% confidence intervals calculated from a bootstrap procedure). Maximum at time lag 0 is always zero (and thus hidden by the origin).

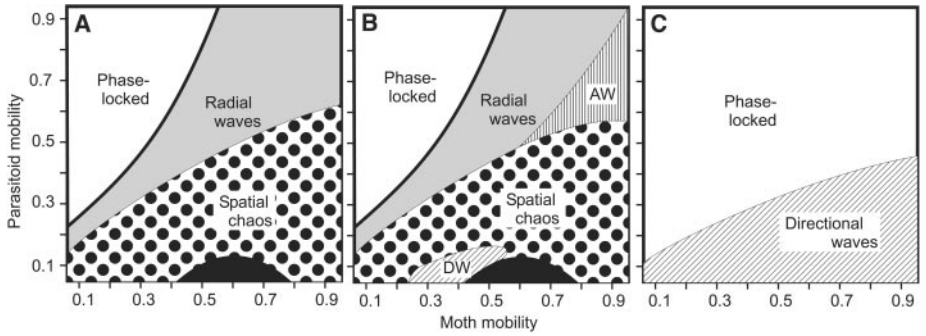

Fig. 4. The relationship between host and parasitoid dispersal and spatial dynamics with (**A**) nondirectional (isotropic) dispersal, (**B**) 30% anisotropy (west-east) in the dispersal of the moth, and (**C**) gradient in habitat quality (r_0 varies clinally and is 10% lower in the "eastern" area) and isotropic dispersal. The white area represents region-wide synchronization. The black area in (A) and (B) represents "partially phase-locked" oscillations, where space is partitioned into a mosaic of phase-locked regions. Diagonal hatching in (B) and (C) represents directional waves ["DW" in (B)]. Note that in (C) the directional waves extend from low-quality areas toward high-quality areas. The area in (B) denoted "AW" represents radial waves that have a tendency toward antidirectional waves in abundance flowing counter to the advection (*18*).

References and Notes

1. R. M. May, *Proc. R. Soc. London Ser. B* **228**, 241 (1986).
2. O. N. Bjørnstad, B. T. Grenfell, *Science* **293**, 638 (2001).
3. M. P. Hassell, H. N. Comins, R. M. May, *Nature* **353**, 255 (1991).
4. J. D. Murray, *Mathematical Biology* (Springer-Verlag, New York, ed. 2, 1993).
5. J. Bascompte, R. V. Solé, Eds., *Modeling Spatiotemporal Dynamics in Ecology* (Springer-Verlag, New York, 1998).
6. W. S. C. Gurney, A. R. Veitch, I. Cruickshank, G. McGeachin, *Ecology* **79**, 2516 (1998).

7. N. Shigesada, K. Kawasaki, *Biological Invasions: Theory and Practice* (Oxford Univ. Press, New York, 1997).
8. A. Hastings, S. Harrison, K. McCann, *Proc. R. Soc. London Ser. B* **264**, 1837 (1997).
9. J. L. Maron, S. Harrison, *Science* **278**, 1619 (1997).
10. W. G. Wilson, S. P. Harrison, A. Hastings, K. McCann, *J. Anim. Ecol.* **68**, 94 (1999).
11. E. Ranta, V. Kaitala, J. Lindström, *Ecography* **20**, 454 (1997).
12. D. T. Haydon, *Theor. Popul. Biol.* **58**, 239 (2000).
13. P. J. Bacon, *Population Dynamics of Rabies in Wildlife* (Academic Press, London, 1985).
14. B. T. Grenfell, O. N. Bjørnstad, J. Kappey, *Nature* **414**, 716 (2001).
15. W. Baltensweiler, *Oecologia* **94**, 62 (1993).
16. _____, D. Rubli, *Forest Snow Landscape Res.* **74**, 1 (1999).
17. C. Auer, *Eidg. Anst. Forstl. Versuchswes. Mitt.* **53**, 71 (1977).
18. See supplemental data on *Science* Online.
19. W. Baltensweiler, *Eidg. Anst. Forstl. Versuchswes. Ber.* **270**, 215 (1985).
20. We analyzed outbreak data that originated from maps of visually detected defoliation in the Central European Alps between 1961 and 1998 (*16*). The surveys were made in cooperation with the forest administration agencies of the Alpine countries (France, Italy, Switzerland, and Austria). Maps were digitized to show the presence or absence of defoliation in each 1 km × 1 km cell. These data were aggregated to the proportion of defoliation in 20 km × 20 km grid cells as a surrogate for local abundance (*18*). Grid cells were excluded from further analyses if the maximum defoliation was less than 1% or if >90% of the years were completely without defoliation. This was done to prevent problems arising from analysis of time series dominated by zero values.
21. O. N. Bjørnstad, J. Bascompte, *J. Anim. Ecol.* **70**, 924 (2001).
22. O. N. Bjørnstad, W. Falck, *Environ. Ecol. Statist.* **8**, 53 (2001).
23. The cross-correlation, $w_{ij,\Delta}$, between two time series of abundance at location H_i and at location i and H_j at location j (either at similar or different locations) lagged by Δ years relative to each other (either in the same year, $\Delta = 0$, or in lagged years), is given by

$$w_{ij,\Delta} = (\underline{H_i} - \langle H_i \rangle) \times (\underline{H_{j,\Delta}} - \langle H_j \rangle)^{\mathrm{T}} / \sigma_{H_i} \sigma_{H_j} \qquad (1)$$

where $\langle H_\cdot \rangle$ represents the mean of the time series, $\sigma_{H_\cdot}$ represents the standard deviations, underscored symbols represent vectors (time series), × denotes matrix multiplication, and the superscript T denotes matrix transposition. The correlation depends on the spatial distance and direction separating the populations, $r_{ij,\theta}$. We thus measure the distance as the projections onto a sequence of cardinal directions $\{\theta: 0, \pi/16, \ldots, 31\pi/32\}$ (*28*) according to $r_{ij,\theta} = x_i \sin(\theta) + y_i \cos(\theta) - x_j \sin(\theta) - y_j \cos(\theta)$. By extension of existing methods (*21*), we estimate the LCCF as a function of direction and time lag as the kernel regression of cross-correlation on directional distance:

$$\tilde{C}(r_\theta, \Delta) = \frac{\sum_{i=1}^{n} \sum_{j=i+1}^{n} K(r_{ij,\theta}/h) w_{ij,\Delta}}{\sum_{i=1}^{n} \sum_{j=i+1}^{n} K(r_{ij,\theta}/h)} \qquad (2)$$

Hence, we estimate spatial correlation for time lags of 0, 1, and 2 years and distance lags up to ±600 km. An R/S-plus library for calculating the metrics is available upon request (onb1@psu.edu).
24. M. P. Hassell, *The Dynamics of Arthropod Predator-Prey Systems* (Princeton Univ. Press, Princeton, NJ, 1978).
25. P. Turchin, *Complex Population Dynamics: A Theoretical/Empirical Synthesis* (Princeton Univ. Press, Princeton, NJ, 2002).
26. The local dynamics of location i of the moth, H_i, and its parasitoid, P_i, are given as a density-dependent version of the Nicholson-Bailey model

$$H'_{i,t+1} = H_{i,t} \exp\left\{ r_{i,0} \left[1 - \left(\frac{H_{i,t}}{K} \right) \right] \right\} \exp\left(\frac{-aP_{i,t}}{1 + awP_{i,t}} \right) \qquad (3)$$

$$P'_{i,t+1} = H_{i,t} \left[1 - \exp\left(\frac{-aP_{i,t}}{1 + awP_{i,t}} \right) \right] \qquad (4)$$

where $H_{i,t}$ is the density of hosts at generation t, $P_{i,t}$ is the density of parasitoids at generation t, $r_{i,0}$ is per capita rate of population change at location i, K is carrying capacity, a is parasitoid search efficiency, and w is a conversion constant. We used the following parameters (*25*): $a = 2.5$, $w = 0.17$, and $K = 250$. In the habitat homogeneous case, $r_{i,0} = 2.5$ for all populations. In the heterogeneous case, $r_{i,0}$ is distributed along a gradient across the lattice from 2.3 to 2.5. A fraction μ_h of adult hosts and a fraction μ_p of adult parasitoids are assumed to disperse into the eight surrounding patches (*3*). The equations for the dispersal stage can be written as

$$H_{i,t+1} = (1 - \mu_h) H'_{i,t+1} + \mu_h \overline{H}'_{i,t+1} \qquad (5)$$

$$P_{i,t+1} = (1 - \mu_p) P'_{i,t+1} + \mu_p \overline{P}'_{i,t+1} \qquad (6)$$

where $H_{i,t+1}$ and $P_{i,t+1}$ denote the post-dispersal abundance of moths and parasitoids at patch i, and $H'_{i,t}$ and $P'_{i,t}$ denote predispersal abundances. The quantities $\overline{H}$ and $\overline{P}$ are the neighborhood host and parasitoid densities (over the eight nearest neighboring patches). The lattice is assumed to have absorbing boundaries. We discarded the first 2000 generations of each simulation; the spatiotemporal patterns from the last 500 generations were then analyzed using the same method as used in the larch budmoth data analysis. The local dynamics for the moth-plant quality model are identical to those in the model proposed by Turchin (*25*). The moth dispersal stage is again modeled according to Eq. 5.
27. O. N. Bjørnstad, R. A. Ims, X. Lambin, *Trends Ecol. Evol.* **14**, 427 (1999).
28. X. Lambin, D. A. Elston, S. J. Petty, J. L. MacKinnon, *Proc. R. Soc. London Ser. B* **265**, 1491 (1998).

29. Supported by USDA, the Academy of Finland, and the National Center for Ecological Analysis and Synthesis (funded by NSF, the University of California, and UC Santa Barbara). We thank A. Satake, P. Tobin, and three anonymous reviewers for comments on earlier versions of the manuscript.

Supporting Online Material

www.sciencemag.org/cgi/content/full/298/5595/1020/DC1

Figs. S1 to S4

18 June 2002; accepted 22 August 2002

Microbial Dehalorespiration with 1,1,1-Trichloroethane

Baolin Sun,[1] Benjamin M. Griffin,[1,2] Héctor L. Ayala-del-Río,[1,2] Syed A. Hashsham,[1,3] James M. Tiedje[1,2]*

1,1,1-Trichloroethane (TCA) is a ubiquitous environmental pollutant because of its widespread use as an industrial solvent, its improper disposal, and its substantial emission to the atmosphere. We report the isolation of an anaerobic bacterium, strain TCA1, that reductively dechlorinates TCA to 1,1-dichloroethane and chloroethane. Strain TCA1 required H_2 as an electron donor and TCA as an electron acceptor for growth, indicating that dechlorination is a respiratory process. Phylogenetic analysis indicated that strain TCA1 is related to gram-positive bacteria with low DNA G+C content and that its closest relative is *Dehalobacter restrictus*, an obligate H_2-oxidizing, chloroethene-respiring bacterium.

TCA is a synthetic organic solvent widely used in industrial processes and is a major environmental pollutant commonly found in soil (*1*), groundwater (*2*), and the atmosphere (*3*). TCA is present in at least 696 of the 1430 National Priorities List sites identified by the U.S. Environmental Protection Agency (EPA) (*1*). Because of TCA's adverse effects on human health, the EPA has set a maximum contaminant level of 200 μg/liter in drinking water (*4*). TCA is also listed as an ozone-depleting substance by the United Nations Environment Programme (*5*). Even when released to soil or leached to groundwater, the primary environmental fate of TCA is volatilization to the atmosphere, where it interacts with ozone and contributes to the erosion of the ozone layer (*1*, *5*). TCA is often a co-contaminant in aquifers with chlorinated ethenes, especially tetrachloroethene (PCE) and trichloroethene (TCE), because they have similar industrial uses. Although in situ bioremediation processes for the chloroethenes are known (*6*), TCA remediation remains problematic and can prevent site restoration.

TCA undergoes slow abiotic degradation to acetic acid and 1,1-dichloroethene, an EPA priority pollutant (*7*). Biotransformation of TCA has been observed under aerobic and anaerobic conditions only in cometabolic processes (*8–11*). A growth-linked, or dehalorespiratory, process would be more effective for in situ bioremediation of TCA-contaminated sites, because reaction rates would be faster and natural selection would ensure growth in situ.

Although bacterial growth by dehalorespiration of chloroethenes, chlorobenzenes, 3-chlorobenzoate, and 2-chlorophenol has been well documented (*12–15*), bacterial growth by reductive dechlorination of TCA has not been reported until now. We describe the isolation of a bacterium capable of energy

[1]Center for Microbial Ecology, [2]Department of Microbiology and Molecular Genetics, [3]Department of Civil and Environmental Engineering, Michigan State University, East Lansing, MI 48824–1325, USA.

*To whom correspondence should be addressed. E-mail: tiedjej@msu.edu